Atmos. Meas. Tech., 6, 3313–3323, 2013
www.atmos-meas-tech.net/6/3313/2013/
doi:10.5194/amt-6-3313-2013

Atmospheric Measurement Techniques Open Access

Multispectral information from TANSO-FTS instrument – Part 2: Application to aerosol effect on greenhouse gas retrievals

H. Herbin, L. C.-Labonnote, and P. Dubuisson

Laboratoire d'Optique Atmosphérique (LOA), UMR8518, Université de Lille 1, 59655 Villeneuve d'Ascq cedex, France

Correspondence to: H. Herbin (herve.herbin@univ-lille1.fr)

Received: 14 November 2012 – Published in Atmos. Meas. Tech. Discuss.: 26 November 2012
Revised: 4 October 2013 – Accepted: 7 October 2013 – Published: 28 November 2013

Abstract. This article is the second in a series of studies investigating the benefits of multispectral measurements to improve the atmospheric parameter retrievals. In the first paper, we presented an information content (IC) analysis from the thermal infrared (TIR) and shortwave infrared (SWIR) bands of Thermal And Near infrared Sensor for carbon Observations–Fourier Transform Spectrometer (TANSO-FTS) instrument dedicated to greenhouse gas retrieval in clear sky conditions. This second paper presents the potential of the spectral synergy from TIR to visible for aerosol characterization, and their impact on the retrieved CO_2 and CH_4 column concentrations. The IC is then used to determine the most informative spectral channels for the simultaneous retrieval of greenhouse gas total columns and aerosol parameters. The results show that a channel selection spanning the four bands can improve the computation time and retrieval accuracy. Therefore, the spectral synergy allows obtaining up to almost seven different aerosol parameters, which is comparable to the most informative dedicated instruments. Moreover, a channel selection from the TIR to visible bands allows retrieving CO_2 and CH_4 total columns simultaneously in the presence of one aerosol layer with a similar accuracy to using all channels together to retrieve each gas separately in clear sky conditions.

1 Introduction

Satellite observations of the earth allow continuous monitoring of the atmosphere from local to global scale. Among them, passive remote sensing instruments, which span a broad frequency range from UV to microwave, provide lots of different information on gas, cloud or aerosol atmospheric composition. Although major efforts have been made from dedicated sounders and modeling, many atmospheric constituents are, up to now, estimated with large uncertainties. In particular, aerosols, which have a high spatiotemporal variability and physico-chemical diversity, remain the largest uncertainty in radiative forcing as well as a source of biases in the greenhouse gas retrieval.

The single channel and viewing angle radiometric observations such as from the Advanced Very High Resolution Radiometer (AVHRR) (Mishchenko et al., 1999; Ignatov, 2002) provide only an estimated value of the aerosol optical depth (AOD). Multi-channel instruments such as MODIS (Tanré et al., 1996) or OMI (Veihelmann et al., 2007) provide between 2 and 4 degrees of freedom for signal (DOFSs) attributed to aerosol parameters (e.g., aerosol optical depth, Ångström exponent, single scattering albedo) using a priori information for other aerosol parameters such as size distribution, or refractive index. The aerosol information content is significantly larger for instruments that perform measurements at multiple viewing angles, such as the MISR (Diner et al., 1999) and AATSR (Veefkind et al., 1999), or multi-wavelength polarized radiances such as GOME-II. Since the light polarization is very sensitive to the aerosol microphysics (Hansen and Travis, 1974), Hasekamp and Landgraf (2005) have shown that 6 to 8 DOFSs can be reached from GOME-II, giving access to the aerosol loading of fine and coarse modes, the effective radius of at least one mode, the real and imaginary part of the refractive index, and the mean height of the aerosol layer. The multi-channel polarized measurements at multiple viewing angles have been shown to be the most efficient way for the aerosol characterization (Lebsock et al., 2007). However, actually only the PARASOL instrument exploits this technique (Deuzé et al., 2000,

2001). Moreover, the latter operates only in the visible spectral range. Thus their retrieved aerosol parameters can hardly be extrapolated in the infrared.

The high spectral resolution infrared sounders are obviously designed to the gaseous species retrieval. Nevertheless, these instruments have the advantage, among others, of being highly sensitive to the aerosol type. Recently, many works have been achieved from infrared spectrometers such as AIRS and IASI (Pierangelo et al., 2004, 2005; De Souza-Machado, 2006; Klüser et al., 2011, 2012; Clarisse et al., 2010, 2013; Quan et al., 2013; Peyridieu et al., 2013). The aerosol characteristics (AOD, mean altitude and size) obtained from infrared appear to be very promising to complement the aerosol parameters retreived from visible observations. The other reason to retrieve a better estimate of the aerosol parameters in the infrared is due to the large error or bias induced by their presence in the atmospheric column on gaseous retrieval. Therefore, several studies on the Thermal And Near infrared Sensor for carbon Observations–Fourier Transform Spectrometer (TANSO-FTS) or pre-launch OCO(-2) (Connor et al., 2008; Butz et al., 2009; Frankenberg et al., 2012; Uchino et al., 2012; Guerlet et al., 2013; Oshchepkov et al., 2013) have been conducted to analyze the aerosol sensitivity and its benefit of improving the accuracy of CO_2 and CH_4 retrievals in the shortwave infrared (SWIR) spectral range in a scattering atmosphere.

Here, we present, for the first time, an information content analysis on (1) aerosol parameters, and (2) greenhouse gas columns in the presence of an aerosol layer, considering a high-resolution multispectral observing system. In particular, we discuss the interest of using several spectral bands simultaneously according to the surface type and state vector composition. This synergetic approach is evaluated from the four bands of the TANSO-FTS instrument covering a large spectral range from thermal infrared to visible, thanks to a new radiative transfer algorithm developed at the Laboratoire d'Optique Atmosphérique (LOA).

Since this paper is the second in a series describing the effects of spectral synergy on the atmospheric observations, the basic specifications of the Greenhouse gases Observing SATellite (GOSAT) instrument (Kuze et al., 2009) and the theoretical bases of the information content were outlined already in Part 1 (Herbin et al., 2013) and are not recalled here. Therefore, the paper is organized as follows: Sect. 2 details the forward model, the state vector composition and error description. Section 3 is dedicated to an information content (IC) analysis of the gaseous profiles in the presence of one aerosol layer. The aerosol IC and channel selection are presented in Sect. 4. The benefit of multispectral synergy for simultaneous aerosol and gas retrieval is discussed in Sect. 5. Finally, Sect. 6 summarizes our results and presents perspectives for future applications.

2 The multispectral simulation of TANSO-FTS in the presence of an aerosol layer

2.1 The forward model

Accurate calculations of the radiances observed by TANSO-FTS are achieved with the high spectral resolution (up to $0.0001\,cm^{-1}$) code LBLDOM (Dubuisson et al., 1996, 2005) over the thermal and solar spectral regions (0.2–16 µm). Radiances at the top of the atmosphere are calculated by solving the radiative transfer equation (RTE) in a horizontally homogeneous scattering atmosphere, using the discrete ordinate method (DOM) (Stamnes et al., 1988). Gaseous absorption is calculated with a line-by-line code based on STRANSAC (Scott, 1974) and the HITRAN 2008 database (Rothman et al., 2009). The absorption lines are computed at $0.01\,cm^{-1}$ spectral resolution assuming a Voigt line shape. Absorption continua (H_2O, CO_2, and N_2) are also included from the MT-CKD parameterization (Clough et al., 2005). The solar irradiance database reported by Kurucz (http://kurucz.harvard.edu/sun/irradiance2008/) is used as the incident solar spectrum. The RTE resolution using DOM approach allows taking into account absorption, emission, Rayleigh and multiple scattering processes for aerosol and gaseous species. Aerosols are defined from their optical parameters: optical depth, single scattering albedo and phase function. These parameters are obtained from a Mie scattering code assuming spherical particles with a bi-modal and lognormal distribution. A Lambertian surface is assumed, and the effect of surface polarization is therefore disregarded. The albedos in the SWIR and visible bands are estimated from MODIS Terra product (Moody et al., 2008) and chosen as desert and seawater in order to cover high and weak surface reflectivities, respectively. The corresponding surface emissivity for the thermal infrared (TIR) band is estimated from the MODIS UCSB library (http://www.icess.ucsb.edu/modis/EMIS/html/em.html). We assumed a nadir viewing angle geometry, with a solar zenith angle of 30°. Although the sensitivity is correlated to viewing geometry, this assumption does not alter results or the discussion of the present study. The total intensities of TANSO-FTS spectra are simulated using the instrumental line shape (ILS) provided for all four bands by the GOSAT user interface gateway (https://data.gosat.nies.go.jp/gateway/gateway/MenuPage/open.do), and no post-apodization is applied, which allows the exploitation of the full spectral resolution.

2.2 The state vector and error definition

The IC analysis is performed on TANSO-FTS simulated unpolarized radiances for Band 1 (visible), Bands 2 and 3 (SWIR), and Band 4 (TIR). The O_2, CO_2 and CH_4 vertical concentrations of the a priori state vector $\boldsymbol{x}_a$ are based on US standard profile discretized on 21 vertical levels, extending from the ground to 20 km height with 1 km step. In order to

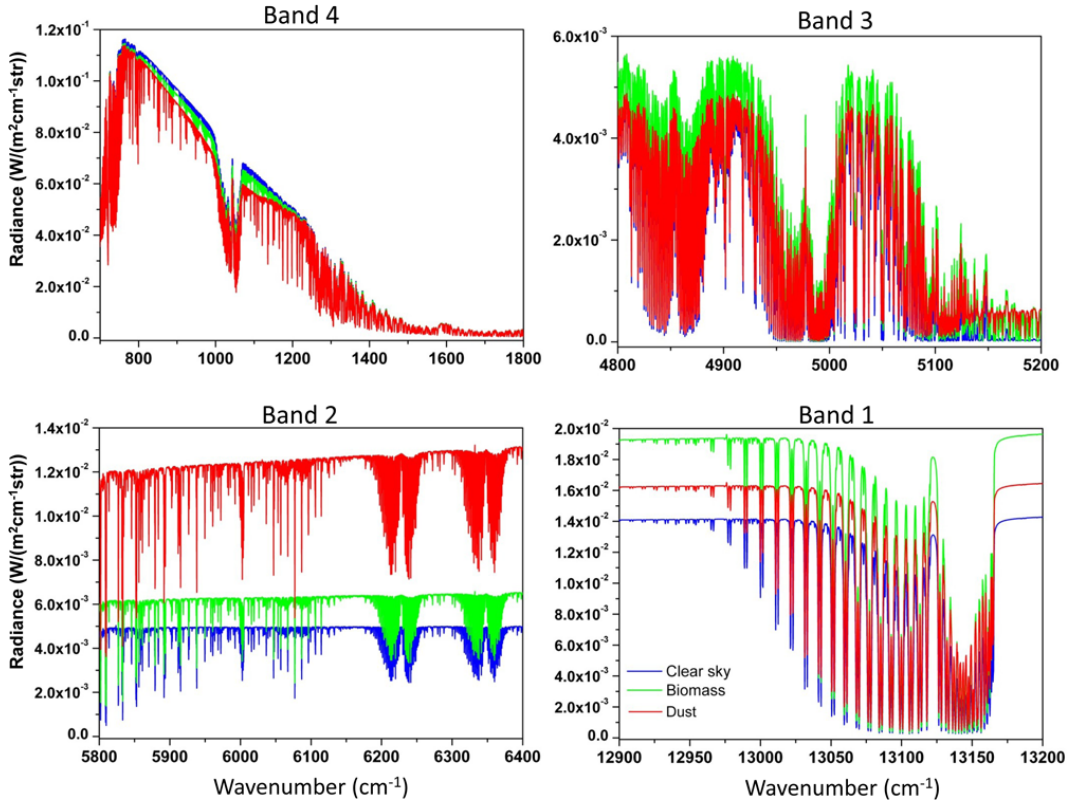

Fig. 1. Simulated TANSO-FTS spectra in radiances (W/(m^2 cm^{-1}str)) for clear sky conditions (blue lines), in the presence of biomass burning particles (green lines) with $\tau_{(440\ \mathrm{nm})} = 0.55$, and dust (red lines) with $\tau_{(1020\ \mathrm{nm})} = 0.25$. Each band is calculated from our line-by-line forward model on US standard profile with nadir viewing angle and solar zenith angle of 30°.

reflect the natural diversity in terms of atmospheric aerosols, we used the general properties of two different aerosol types: dust and biomass burning particles, which are the most common tropospheric aerosol. The aerosol microphysical properties are described by seven state vector elements derived from Dubovik et al. (2002) climatology as follows: total optical depth (τ), which is the sum of the fine- and coarse-mode optical depth calculated from particle concentration C (in part m^{-3}), the altitude and geometrical thickness of the aerosol layer, mean radius r (in µm) and standard deviation logarithm ln(σ) for fine and coarse mode (subscripted f and c, respectively). Moreover, we assumed one homogeneous aerosol layer with a 2 km geometrical thickness, located between 3–5 km for biomass burning and 7–9 km for dust. In addition, the humidity and temperature profile, surface reflectivity, TIR surface emissivity, and the real and imaginary parts of the refractive index are treated as non-retrieved parameters and are discussed in detail in Sect. 2.2.3. All the a priori values and their a priori variabilities are summarized in Table 1 and are described subsequently hereafter. The radiance spectra for each TANSO-FTS band, illustrated in Fig. 1, are computed from our forward model with refractive index coming from Sutherland and Khanna (1991) for biomass particles, and from Volz (1973) for sand dust, assuming a bi-modal lognormal distribution and an aerosol optical depth (AOD) of $\tau_{(440\ \mathrm{nm})} = 0.55$ and $\tau_{(1020\ \mathrm{nm})} = 0.25$, respectively.

As stated in the first paper (Herbin et al., 2013), two matrices (**A** and $\mathbf{S}_x$) allow a full characterization of the information provided by the observing system.

A, which is the averaging kernel matrix, gives a measure of the sensitivity of the retrieved state to the true state, and is defined by

$$\mathbf{A} = \partial \hat{\boldsymbol{x}} \big/ \partial \boldsymbol{x} = \mathbf{GK}, \tag{1}$$

where **K** is the Jacobian matrix, given by $\mathbf{K} = (\partial F \big/ \partial \boldsymbol{x})$, the gain matrix whose rows are the derivatives of the retrieved state with respect to the spectral points is defined by

$$\mathbf{G} = \partial \hat{\boldsymbol{x}} \big/ \partial \boldsymbol{y} = (\mathbf{K}^{\mathrm{T}} \mathbf{S}_{\varepsilon} \mathbf{K} + \mathbf{S}_a^{-1})^{-1} \mathbf{K}^T \mathbf{S}_{\varepsilon}^{-1}, \tag{2}$$

where $\mathbf{S}_a$ is the error covariance matrix describing our knowledge of the state space prior to the measurement, and $\mathbf{S}_{\varepsilon}$ represents the forward model and the measured signal error covariance matrix.

At a given level, the peak of the averaging kernel row gives the altitude of maximum sensitivity, whereas its full width at half maximum is an estimate of the vertical resolution. Rodgers (2000) demonstrated that the trace of **A** represents

Table 1. Summary of assumed aerosol parameters adapted from Dubovik et al. (2002). C is number of particles in part m^{-3}, r mean radius in µm, and σ deviation of the radius in µm. The f and c indices are for fine and coarse mode respectively. $\tau_{(1020)}$ and $\tau_{(440)}$ correspond to the optical depth at 1020 and 440 nm, respectively.

	Dust	Biomass	Paw (%)
Real refractive index	Volz (1973)	Sutherland and Khanna (1991)	10
Imaginary refractive index	Volz (1973)	Sutherland and Khanna (1991)	10
Fine-mode concentration, C_f (part m^{-3})	$1.58 \times 10^9 + 7.92 \times 10^9 \tau_{(1020)}$	$6.97 \times 10^7 \tau_{(440)}/r_f^3$	100
Fine-mode radius, r_f (µm)	0.088	$0.087+8 \times 10^{-3} \tau_{(440)}$	100
Fine-mode deviation, $\ln(\sigma_f)$	0.42	0.40	100
Coarse-mode concentration, C_c (part m^{-3})	$-7.8 \times 10^5 + 3.573 \times 10^7\ \tau_{(1020)}$	$3.598 \times 10^5 \tau_{(440)}/r_c^3$	100
Coarse-mode radius, r_c (µm)	0.832	$0.503 + 0.089\ \tau_{(440)}$	100
Coarse-mode deviation, $\ln(\sigma_c)$	0.61	0.79	100
Aerosol center height (km)	8	6	50
Aerosol layer width (km)	2	2	100
O_2	US standard		0.2

the total degrees of freedom for signal (DOFSs), which indicate the amount of independent pieces of information provided by the observing system as regards the state vector.

The error covariance matrix $\mathbf{S}_x$ describes the knowledge of the state space posterior to the measurement. Rodgers (2000) demonstrated that this error covariance matrix can be written as

$$\mathbf{S}_x = \mathbf{S}_{\text{smoothing}} + \mathbf{S}_{\text{meas.}} + \mathbf{S}_{\text{fwd.mod.}}, \quad (3)$$

where $\mathbf{S}_{\text{smoothing}}$ is the smoothing error covariance matrix and represents the vertical sensitivity of the measurements to the retrieved profile. The latter is given by

$$\mathbf{S}_{\text{smoothing}} = (\mathbf{A} - \mathbf{I})\mathbf{S}_a(\mathbf{A} - \mathbf{I})^{\mathrm{T}}. \quad (4)$$

$\mathbf{S}_{\text{meas.}}$ is the contribution of the measurement error covariance matrix $\mathbf{S}_m$ associated with the spectral noise, and is given by

$$\mathbf{S}_{\text{meas.}} = \mathbf{G}\mathbf{S}_m\mathbf{G}^{\mathrm{T}}. \quad (5)$$

$\mathbf{S}_{\text{fwd.mod.}}$ is the contribution of the forward model error covariance matrix $\mathbf{S}_f$ associated with uncertainties from non-retrieved model parameters expressed by the covariance matrix $\mathbf{S}_b$.

$$\mathbf{S}_{\text{fwd.mod.}} = \mathbf{G}\mathbf{K}_b\mathbf{S}_b(\mathbf{G}\mathbf{K}_b)^{\mathrm{T}} = \mathbf{G}\mathbf{S}_f\mathbf{G}^{\mathrm{T}}, \quad (6)$$

where $\mathbf{K}_b$ is the forward model derivative as regards non-retrieved model parameters ($\boldsymbol{x}_b$), and $\mathbf{S}_b$ the error covariance matrix attached to $\boldsymbol{x}_b$.

2.2.1 A priori error covariance matrix

To be consistent with the first paper (Herbin et al., 2013), the a priori error covariance matrix $\mathbf{S}_a$ is assumed diagonal with the ith diagonal element ($S_{a,ii}$) defined as

$$S_{a,ii} = \sigma_{a,i}^2 \ \text{ with } \ \sigma_{a,i} = x_{a,i}.\frac{p_{\text{error}}}{100}, \quad (7)$$

where $\sigma_{a,i}$ stands for the standard deviation in the Gaussian statistics formalism. The subscript i represents the ith parameter of the state vector.

In order to take into account their influence on the information and errors about the gas column, we have to specify the uncertainty of each aerosol parameter needed in the forward model computation (e.g., to compute the matrix $\mathbf{S}_b$). The prior knowledge of aerosol parameters ($\mathbf{C}$, $\boldsymbol{r}$, $\ln(\sigma)\Delta Z$) is supposed to be known with an uncertainty of Paw = 100 % (Frankenberg et al., 2012), and 50 % for aerosol layer center height (Z_m). The prior knowledge of the other atmospheric parameters are identical to the first paper and are recalled in Table 2. The CO_2 profile a priori error is estimated from Schmidt and Khedim (1991) and is very similar to the one used by Christi and Stephens (2004). The CH_4 a priori error is fixed to $P_{\text{error}} = 5$ % (see Eq. 7), which corresponds to an under-constrained version of the error covariance matrix used by Razavi et al. (2009).

2.2.2 Measurement error covariance matrix

In order to compute the measurement error covariance matrix, we need to estimate the radiometric calibration and radiometric noise, usually given as a signal-to-noise ratio (SNR). This error covariance matrix is assumed to be diagonal, and the ith diagonal element can be computed as follows:

$$S_{m,ii} = \sigma_{m,i}^2 \ \text{ with } \ \sigma_{m,i} = \frac{y_i}{\text{SNR}}, \quad (8)$$

where $\sigma_{m,i}$ is the standard deviation of the ith measurement (y_i) of the measurement vector $\boldsymbol{y}$, representing the noise equivalent spectral radiance. For the TIR Band 4, the SNR is estimated as 300 for a 280 K blackbody light input (Kuze et al., 2009). For the SWIR and visible bands, we have applied an identical SNR. The latter is estimated from the Band 2 SNR values given by Yoshida et al. (2011). According to the different surfaces types, the SNR was set to 500 and 150,

Table 2. State vector parameters.

State vector elements	H_2O	CO_2	CH_4	Interfering species	Surface temperature	Profile temperature	Emissivity/ reflectivity
A priori values ($\boldsymbol{x}_a$)	US standard						MODIS database
A priori uncertainty (P_{error})	10 %	1.3–8 %	5 %	100 %	1 K	1 K/layer	2 %

representative of high (desert-like) and low (seawater-like) surface reflectivity cases.

2.2.3 Non-retrieved parameter characterization and accuracy

For the temperature profile and surface temperature, we assumed a realistic uncertainty of 1 K ($\Delta T = 1$ K), compatible with the typical values used for the ECMWF assimilation, on each layer of the temperature profile as well as on surface temperature. The contribution to the ith diagonal element of the forward model error covariance matrix from the jth level temperature can be computed as

$$\sigma_{\text{f},T_j,i} = \frac{\partial F_i}{\partial T_j}\Delta T, \tag{9}$$

where j stands for the jth level and i for the ith measurement.

The surface emissivity (ε_m) uncertainty is set to $P_{\varepsilon_m} = 2\,\%$, which corresponds to an average value of the albedo absolute accuracy from MODIS and IASI (Capelle et al., 2012), and its contribution to the ith diagonal element of the forward model error covariance matrix is

$$\sigma_{\text{f},\varepsilon,i} = \frac{\partial F_i}{\partial \varepsilon}\Delta\varepsilon, \text{ with } \Delta\varepsilon = \frac{p_\varepsilon}{100}\varepsilon_m. \tag{10}$$

The O_2 a priori error is fixed to $P_{CO_2} = 0.2\,\%$, which corresponds to the prior variability used by Frankenberg et al. (2012). H_2O is assumed to be known from ancillary data, and its a priori error profile is set to $P_{CH_2O} = 10\,\%$. This error value is compatible with typical a posteriori uncertainties from operational Level 2 products of a dedicated instrument such as IASI (Clerbaux et al., 2007).

For the other interfering molecule concentrations, we consider a weak prior knowledge, and their uncertainties (P_{Cmol}) are fixed to 100 %. The prior contribution to the ith diagonal element of the forward model error covariance matrix can be computed as

$$\sigma_{\text{f},c_{\text{mol}^k},i} = \frac{\partial F_i}{\partial c_{\text{mol}^k}}\Delta c_{\text{mol}^k}, \text{ with } \Delta c_{\text{mol}^k} = \frac{p_{\text{Cmol}}}{100}c_{\text{mol}^k}, \tag{11}$$

where C^k_{mol} represents the concentration of the kth interfering molecule in ppmv.

The real and imaginary parts of the refractive index are considered with a priori uncertainties of 10 %. The latter is suitable, for instance, if we consider that we know the aerosol type, but not exactly the mineralogical composition. Its contribution to the ith diagonal element of the model parameter error covariance matrix is as for the other non-retrieved parameters:

$$\sigma_{\text{f},m_x,i} = \frac{\partial F_i}{\partial m_x}\Delta m_x, \text{ with } \Delta m_x = \frac{p_{m_x}}{100}m_x, \tag{12}$$

where the subscript x stands for the real part and imaginary parts of the refractive index.

Finally, the total forward model parameter error covariance matrix ($\mathbf{S}_\text{f}$), assumed diagonal in the present study, is given by summing all these error contributions for each diagonal element, and the ith diagonal element ($S_{\text{f},ii}$) is given by

$$S_{\text{f},ii} = \sum_{j=1}^{n\text{level}}\sigma^2_{\text{f},T_j,i} + \sum_{k=1}^{n\text{molecules}}\sigma^2_{\text{f},c_{\text{mol}^k},i} + \sum_{x=r}^{j}\sigma^2_{\text{f},m_x,i} + \sigma^2_{b,\varepsilon,i}. \tag{13}$$

Here, we did not consider the spectroscopic line parameter, line-mixing, continua or calibration errors.

3 Greenhouse gas IC analysis in the presence of aerosols

It is notoriously known that the clear sky observations are only a small part of the entire set of measurements (Eguchi and Yokota, 2008). Moreover, the aerosol and/or cloud scattering is a major source of error for greenhouse gas retrievals using backscatter measurements (Frankenberg et al., 2012; Butz et al., 2009; and references therein). The goal of this section is therefore to study the effect of the presence of one aerosol layer on the CO_2 and CH_4 column information content and errors. The aerosol layer parameters are assumed to be known from ancillary data and are treated as nonretrieved parameters, but they are explicitly taken into account in the forward model. To be consistent with the first part of the study (Herbin et al., 2013), the IC analysis is based on the 694 most informative channels representative of the desert and ocean surfaces selected from a channel selection procedure in clear sky conditions. In this particular case, the model parameter error covariance matrix ($\mathbf{S}_\text{f}$) has to be updated with uncertainties on aerosol parameters in order to understand the

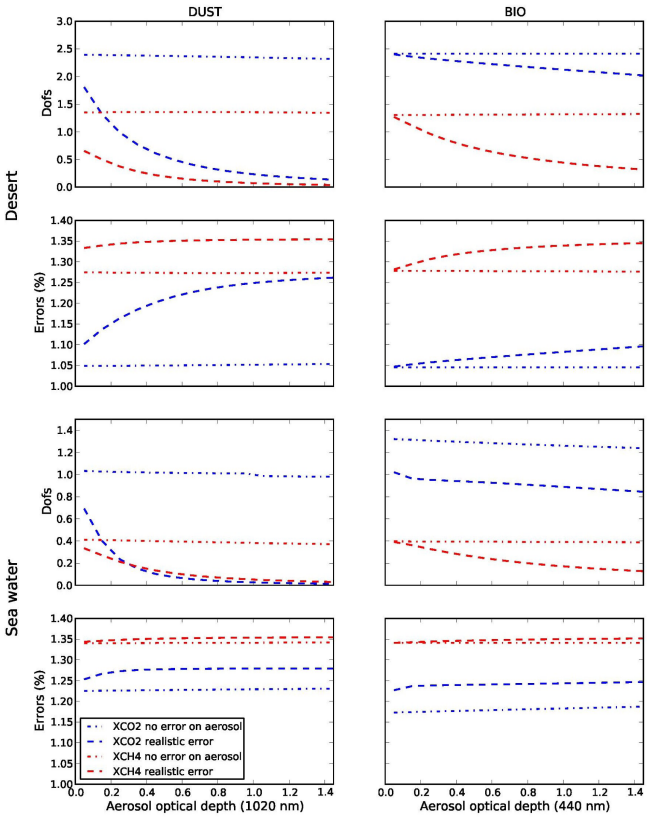

Fig. 2. Gaseous column DOFSs and errors (in %) vs. AOD. CO_2 is in blue lines and CH_4 is in red lines. Case 1 and Case 2 are dotted and dashed lines, respectively.

impact of aerosol parameters on the error budget and information content of gas column concentration. We need therefore to update Eq. (13) by adding the following error contribution to $S_{f,ii}$:

$$\sum_{w=1}^{n\text{para}} \sigma^2_{\text{f},a_w,i} \text{ where } \sigma_{\text{f},a_w,i} = \frac{\partial F_i}{\partial a_w}\Delta a_w \text{ and } \Delta a_w = \frac{p_{a_w}}{100}a_w. \quad (14)$$

Here a_w stands for the wth aerosol parameter.

Figure 2 shows the DOFSs and errors on CO_2 and CH_4 columns as a function of aerosol optical thickness (τ) from 0.05 to 1.45. This figure aims at illustrating information and error sensitivity of greenhouse gas column to aerosol type and loading. In the present study two cases are considered: (1) the aerosol parameters are assumed to be perfectly known (all $P_{\text{awr}} = 0\,\%$), which is an ideally theoretical case (called Case 1 hereafter); and (2) the uncertainties from Table 1 are used, which represent a realistic case (called Case 2 hereafter). If we compare Case 1 (shown by the dashed-dotted lines) with the clear sky condition results (Herbin et al., 2013), we observe that the presence of aerosol decreases the gaseous information even if the aerosol parameters are perfectly known. This is explained by the fact that, in the presence of an aerosol layer, the Jacobians with respect to CO_2 and CH_4 concentration at each level are weaker, and decrease with increasing aerosol optical depth. The dashed lines, which represent Case 2, show that the IC depends on aerosol optical depth and on aerosol type. For instance, the CO_2 and CH_4 DOFSs are divided by a factor of 2 for AOD of 0.25 in the presence of dust layer whatever the surface and tend to zero for higher AOD. Important to note is that the impact on the gas column errors is limited by the high a priori constraint assumed for each gas. Indeed, the gas column errors increase systematically with AOD, and almost reach the a priori errors computed from the a priori error profile as Herbin et al. (2013) and given by

$$\sigma_{\text{XCO}_2} = \frac{\sqrt{\mathbf{C}_{\text{air}}^{\text{T}} S_{\text{XCO}_2} \mathbf{C}_{\text{air}}}}{\mathbf{C}_{\text{air}}^{\text{T}} \mathbf{1}}, \quad (15)$$

where $\mathbf{C}_{\text{air}}$ is the vector containing the air molecule concentration at each level, and $\mathbf{1}$ is a column vector with unity elements.

These errors are respectively 1.28 % and 1.36 % for CO_2 and CH_4 column concentration. For instance, above seawater, the DOFSs present values less than 1, even for low AOD. This is due to the weak information provided by the measurements from SWIR and visible bands over ocean. In consequence, a retrieval algorithm should converge close to the a priori values ($\boldsymbol{x}_a$), and the a posteriori uncertainty will be limited by the a priori variability, but potentially with large biases.

4 Aerosol IC analysis and channel selection

In this section, we analyze the ability of spectral synergy to get information on microphysical aerosol properties. Therefore, we performed an IC analysis considering all channels from the four bands spanning TIR to visible spectral range, with respect to the seven aerosol state vector elements (Table 1). The analysis is focused on dust and biomass burning particles. The real and imaginary parts of the refractive index are treated as non-retrieved parameters with 10 % uncertainty and are taken into account in the forward model error covariance matrix. This is justified by the following facts: (1) TANSO-FTS is a nadir-only sounder, and it has already been shown that without multi-viewing or polarized information, the real and imaginary part of the refractive index is difficult to determine, and (2) in the TIR band the refractive index is highly variable. Figure 3 shows the DOFS and posterior error evolution with AOD for total aerosol optical depth, mean radius and deviation for coarse and fine mode (r_c, $\ln(\sigma_c)$, r_f, $\ln(\sigma_f)$), mean altitude of the aerosol layer (Z_m) and aerosol layer width (ΔZ). The general trend is that the information on individual aerosol parameters increases with AOD, whatever the surface or particle type. More specifically, the mean aerosol layer height should be almost perfectly retrieved (DOFS $\sim$ 1) in all cases. Moreover,

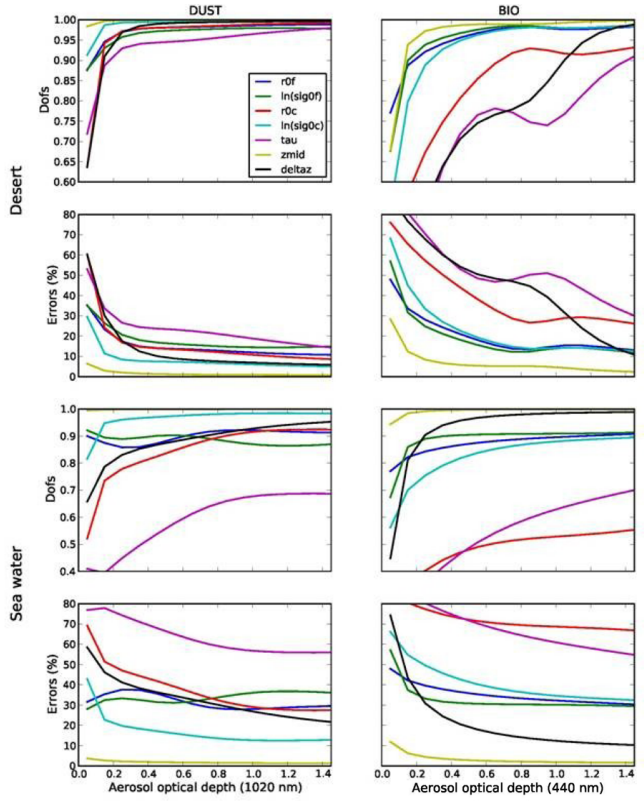

Fig. 3. DOFSs and total error (in %) for each aerosol parameter of the state vector. τ is AOD, r mean radius, and $\ln(\sigma)$ deviation of the radius. The f and c indices are for fine and coarse mode respectively. Z_{mid} and ΔZ are center height and width of the aerosol layer.

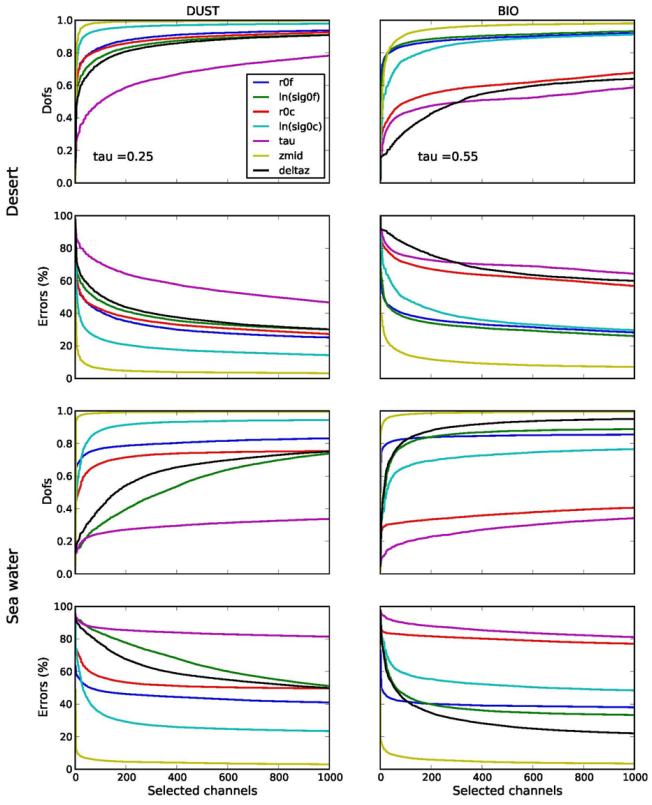

Fig. 4. DOFSs and total error (in %) for each aerosol parameter of the state vector vs. number of selected channels.

the remaining DOFSs are almost always higher than 0.5, indicating that the information on aerosol mostly comes from the measurement. In the worst case (e.g., biomass above sea), the total aerosol parameter DOFS is 5.34 for an aerosol optical depth at 440 nm of 0.55. On the other hand for the best case (e.g., dust above desert), the total DOFS is 6.2 for an optical depth at 1020 nm of 0.25, which means that the observing system should provide enough information to retrieve almost all aerosol parameters. This DOFS is comparable to the best DOFS values obtained from dedicated instruments (see Sect. 1). These results highlight the potential of the TANSO-FTS instrument used in spectral synergy to retrieve aerosol parameters independently.

As stated in the first paper (Herbin et al., 2013), the use of all the channels measured by TANSO-FTS in an inversion scheme has two disadvantages: (1) it requires a huge computational time, and (2) it increases the systematic errors from correlation of the interfering molecules. As emphasis by Rodgers (2000), the SIC framework is very well suited to optimize the selection of channels that carry the greatest amount of information. The channel selection was performed by following the procedure described by L'Ecuyer et al. (2006). Some previous works used the channel selection to optimize the retrievals from high-resolution infrared sounders, and in particular from TANSO-FTS (Herbin et al., 2013; and references therein). However, the channel selection for retrieving aerosol parameters using IC from the TIR to visible spectral range (Bands 4, 3, 2 and 1) is presented here for the first time.

We performed this channel selection considering the state vector elements corresponding to the mean aerosol optical thickness derived from Dubovik et al. (2002): $\tau_{(440\ \mathrm{nm})} = 0.55$ for biomass particles and $\tau_{(1020\ \mathrm{nm})} = 0.25$ for dust. Figure 4 shows the DOFS and error evolution with the number of selected channels from all spectral bands for each surface. We have limited the number of channels to 1000, which corresponds roughly to 90 % of the total information when using all available channels.

For each parameter, the DOFS increases sharply with the first selected channels and then very steadily. It may be noticed that in all cases the information is significantly improved compared to the a priori uncertainties, which are fixed to 50 % for aerosol layer center height (Z_{m}) and 100 % for all other parameters (see Table 1). Therefore, Z_{m} can be systematically retrieved with a good accuracy (posterior error mainly less than 10 %). Nevertheless, the other parameters are estimated with a posterior error between 10 % and 20 % larger than if we had used all the available channels (see Fig. 3). Table 3 gives the number of selected channels needed to reach 75 % of the total information for each aerosol type

Table 3. Number of selected channels for 75 % total IC on aerosol parameters.

	Desert	Seawater	All surfaces
Dust	347	439	652
Biomass	407	222	492

and surface. The last column of Table 3 gives the total number of different channels for all the surfaces. The latter are 652 and 492 for dust and biomass respectively, which correspond to the numbers of channels necessary to obtain 75 % of the total IC. The distributions (in %) by spectral band of the previously selected channels are reported in Table 4. From this Table, we can remark that if the band-by-band distribution of the information is dependent on the aerosol type and surface, the use of all the bands simultaneously appears essential to improve the aerosol parameter retrieval. Table 5 illustrates, in the case of dust above desert, the information distribution by band for each parameter. It can be seen that Band 1 is predominant to retrieve the total aerosol optical depth and the fine-mode granulometry (r_f and $\ln(\sigma_f)$); the coarse-mode granulometry (r_c and $\ln(\sigma_c)$) information is mainly provided by Bands 3 and 4, with the aerosol height (Z_m) and width (ΔZ) parameters coming mostly from Bands 2 and 3. This demonstrates the usefulness of channel selection on multispectral measurements to retrieve the aerosol parameters with a good accuracy and independently of the surface.

5 IC for simultaneous retrieval of gas and aerosol parameters

Section 3 pointed out that one of the major sources of uncertainties concerning the retrieval of gas column in a scattering atmosphere comes from a lack of information about the aerosol parameters. Moreover, the previous section (Sect. 4) has shown that high spectral measurements from the TIR to visible provide information about aerosol microphysics. Therefore, in the present section we study the ability of TANSO-FTS measurements to retrieve simultaneously greenhouse gas total columns and aerosol parameters in order to reduce posterior errors on gas columns. Since the channel selection for aerosol parameters is almost independent of the AOD (not shown here), we performed an IC analysis using the 694 selected channels to get CO_2 and CH_4 simultaneously in clear sky (Herbin et al., 2013), and add the 652 and 492 selected channels from the previous section to obtain dust and biomass particle information.

Figure 5 shows the evolution of DOFSs and associated errors with AOD for each aerosol parameter described in the previous section. In comparison to Fig. 3, the information is higher for each parameter. This is explained by the use of more spectral channels and the improvement of greenhouse gas accuracy.

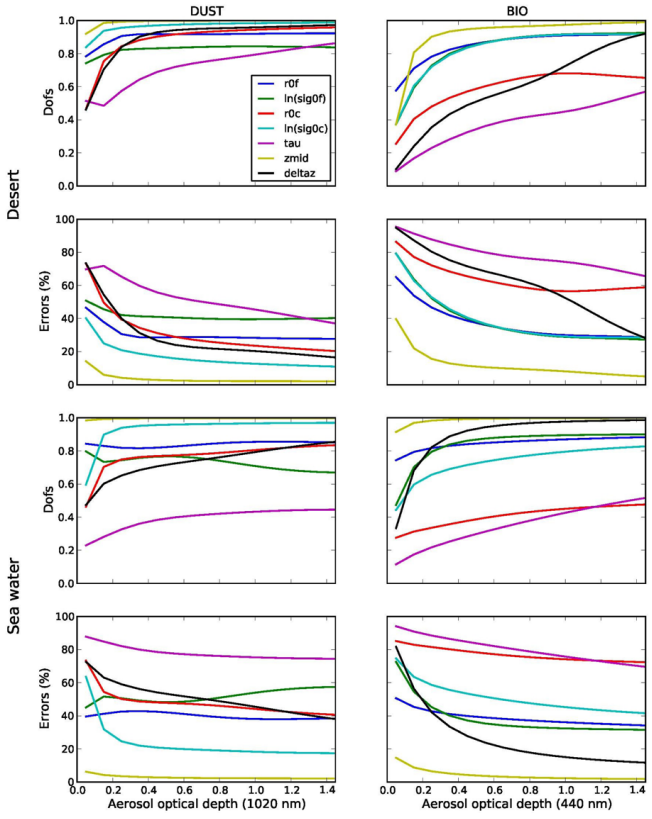

Fig. 5. DOFSs and total error (in %) for each aerosol parameter of the state vector considering selected channels (see text for details). τ is AOD, r mean radius, and $\ln(\sigma)$ deviation of the radius. The f and c indices are for fine and coarse mode respectively. Z_{mid} and ΔZ are center height and width of the aerosol layer.

Figure 6 gives the DOFS and total error evolution on CO_2 (straight blue lines) and CH_4 (straight red lines) column concentrations with AOD. In regards of Fig. 2, we can see that the inclusion of aerosol parameters in the state vector increases significantly and systematically the information on the retrieved gaseous columns. In particular, over desert surface, the total DOFS values are always higher than 1, whatever the AOD. As pointed out previously, this is due to a better knowledge of the aerosol microphysics, which reduces the error coming from the forward model. This is highlighted by the error panels, which show that the posterior uncertainties are now very close to those computed in clear sky conditions.

These results confirm the capabilities of multispectral measurements from TANSO-FTS to retrieve greenhouse gas total columns and up to seven aerosol parameters simultaneously depending on the scene conditions. Moreover, less than 1500 selected channels spanning the four spectral bands from TIR to visible allow retrieving CO_2 and CH_4 column concentration in the presence of an aerosol layer with a similar accuracy to using all the available channels to retrieve each gas separately in clear sky conditions.

Table 4. Band-by-band repartition of selected channels (in %) for aerosol parameter retrieval.

	Dust desert	Dust seawater	Dust all surfaces	Biomass desert	Biomass seawater	Biomass all surfaces
Band 1	44	37	38	27	28	28
Band 2	31	13	24	20	1	17
Band 3	7	16	11	32	55	37
Band 4	18	34	27	21	16	18

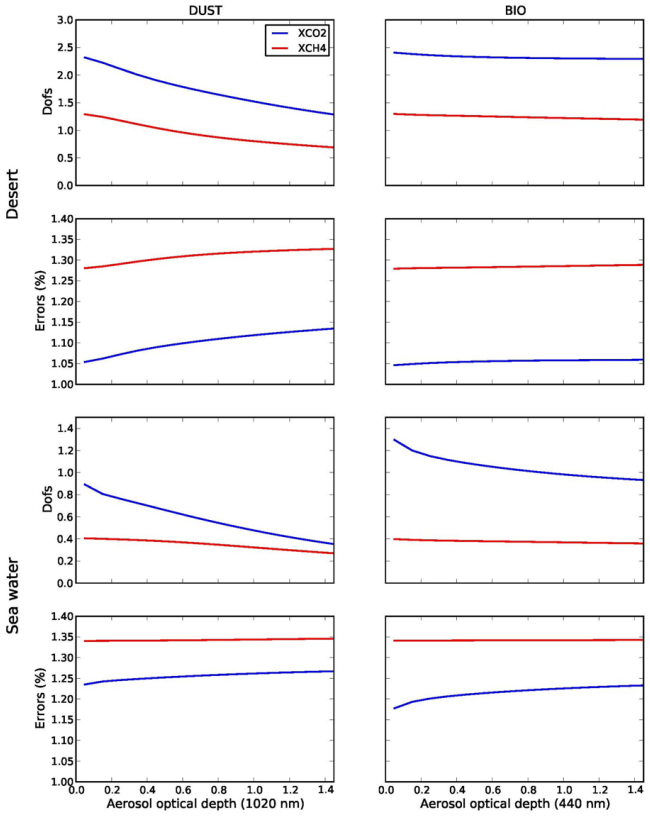

Fig. 6. Gaseous column DOFSs and errors (in %) vs. AOD for channel selection. CO_2 is in blue lines and CH_4 is in red lines.

In this study, the refractive indices are treated as non-retrieved parameters. This implies knowing at least roughly the type of aerosol particle in the measured column. It is obviously a strong constraint of the proposed method, which limits its suitability for operational retrievals. Nevertheless, this limitation is identical for all unpolarized and nadir viewing instruments in the TIR, and can be circumvented, for instance, by using an off-line preprocessing of the aerosol type (see Clarisse et al., 2013).

6 Summary and conclusion

The first part of this paper addresses the question of how the presence of an aerosol layer, in the measured column, impacts the retrieval of CO_2 and CH_4 total columns. The results show that column gas DOFSs are dramatically affected if we have poor aerosol parameter prior knowledge. Moreover, the effect increases with optical depth and strongly depends on aerosol and surface type. Nevertheless, this study also shows that errors in gas columns are less affected by the presence of aerosol if we assume a high constraint on the a priori gas profile concentrations.

Table 5. Band-by-band repartition of IC (in %) for dust particle parameters above desert surface.

	r_f	Ln(σf)	r_c	Ln(σc)	τ	Z_{mid}	ΔZ
Band 1	79	70	17	10	50	27	24
Band 2	6	1	14	9	7	21	42
Band 3	9	18	55	24	33	40	27
Band 4	6	11	14	57	10	12	7

In a second part an IC analysis on aerosol parameters has been conducted to understand the information of such measurements related to the mean radius and variance of the two aerosol modes (r_f, ln(σ_f), r_c, ln(σ_c)), total AOD (τ), mid-altitude (Z_m) and geometrical thickness (ΔZ). The most important result shows that the total aerosol DOFS depends on the surface type and aerosol type. In the worst case (e.g., biomass above ocean), the expected total DOFS is 5.3 (for an average optical depth at 440 nm of 0.55), meaning that the observing system still carries information about the mid-altitude of the layer, the geometrical thickness, the mean radius and width of the coarse mode and width of the small mode with errors smaller than 40 % and less than 5 % for Z_m. In the most favorable case (e.g., dust above desert), the expected total DOFS is equal to 6.2 (for an average optical depth at 1020 nm of 0.25), meaning that almost all parameters should be retrieved with good accuracy. The expected errors for all parameters are below 20 % and below 2 % for Z_m. This is comparable to the best DOFS values obtained from dedicated instruments. These results highlight the potential of the TANSO-FTS instrument to retrieve aerosol parameters with a very good accuracy even above a very dark surface.

Finally, we have selected the best channels with regard to aerosol parameters corresponding to 75 % of the total aerosol IC, merged them with the best channels selected for gas

profiles (see Part 1 – Herbin et al., 2013) and applied an IC on both gas columns together with aerosol parameters. The results show unambiguous improvement of the CO_2 and CH_4 column concentration in the presence of aerosol with an accuracy similar to the one reached in clear sky conditions.

This second paper dedicated to the benefits of multispectral measurements concerns only intensity spectra from TANSO-FTS. In consequence, a future work will focus on the contribution of SWIR and visible polarized bands, in order to address the problem of refractive index retrieval.

Acknowledgements. The authors acknowledge B. Bonnel for his advice on Mie scattering algorithm. This work was supported by the French Space Agency, Centre National d'Etudes Spatiales (CNES), project "GOSAT-TOSCA". We are grateful to the University of Lille local cluster and to the European Grid Infrastructure (EGI) for providing computational resources that have been necessary for this study.

Edited by: M. King

The publication of this article is financed by CNRS-INSU.

References

Butz, A., Hasekamp, O. P., Frankenberg, C., and Aben, I.: Retrievals of atmospheric CO_2 from simulated space-borne measurements of backscattered near-infrared sunlight: accounting for aerosol effects, Appl. Optics, 48, 3322–3336, 2009.

Cappelle, V., Chédin, A., Péquignot, E., Schlüssel, P., Newman, S. M., and Scott, N. A.: Infrared Continental Surface Emissivity Spectra and Skin Temperature Retrieved from IASI Observations over the Tropics, J. Appl. Meteorol. Climate, 51, 1164–1179, 2012.

Christi, M. J. and Stephens, G. L.: Retrieving profiles of atmospheric CO_2 in clear sky and in the presence of thin cloud using spectroscopy from the near and thermal infrared: A preliminary case study, J. Geophys. Res., 109, D04316, doi:10.1029/2003JD004058, 2004.

Clarisse, L., Hurtmans, D., Prata, A. J., Karagulian, F., Clerbaux, C., De Mazière, M., and Coheur, P.-F.: Retrieving radius, concentration, optical depth, and mass of different types of aerosols from high-resolution infrared nadir spectra, Appl. Optics, 49, 3713–3722, 2010.

Clarisse, L., Coheur, P.-F., Prata, F., Hadji-Lazaro, J., Hurtmans, D., and Clerbaux, C.: A unified approach to infrared aerosol remote sensing and type specification, Atmos. Chem. Phys., 13, 2195–2221, doi:10.5194/acp-13-2195-2013, 2013.

Clerbaux, C., Hadji-Lazaro, J., Turquety, S., George, M., Coheur, P.-F., Hurtmans, D., Wespes, C., Herbin, H., Blumstein, D., Tournier, B., and Phulpin, T.: The IASI/MetOp mission: first observations and highlight of its potential contribution to the GMES Earth observation component, Space Res. Today, 168, 19–24, 2007.

Clough, S. A., Shephard, M. W., Mlawer, E. J., Delamere, J. S., Iacono, M. J., Cady-Pereira, K., Boukabara, S., and Brown, P. D.: Atmospheric radiative transfer modeling: a summary of the AER codes, J. Quant. Spectrosc. Radiat. Transfer, 91, 233–244, 2005.

Connor, B. J., Boesch, H., Toon, G., Sen, B., Miller, C., and Crisp, D.: Orbiting Carbon Observatory: Inverse method and prospective error analysis, J. Geophys. Res., 113, D05305, doi:10.1029/2006JD008336, 2008.

De Souza-Machado, S., Strow, L. L., Motteler, H., and Hannon, S.: Infrared dust spectral signatures from AIRS, Geophys. Res. Lett., 33, L03801, doi:10.1029/2005GL024364, 2006.

Deuzé, J.-L., Goloub, P., Herman, M., Marchand, A., Perry, G., and Tanré, D.: Estimate of the aerosols properties over the ocean with POLDER, J. Geophys. Res., 105, 15329–15346, 2000.

Deuzé, L., Bréon, F. M., and Devaux, C.: Remote sensing of aerosols over land surfaces from POLDER-ADEOS–1 polarized measurements, J. Geophys. Res., 106, 4913–4926, 2001.

Diner, D. J., Abdou, W. A., Ackerman, T. P., Crean, K., Gordon, H. R., Kahn, R. A., Martonchik, J. V., McMuldroch, S., Paradise, S. R., Pinty, B., Verstraete, M. M., Wang, M., and West, R. A.: MISR Level 2 Aerosol Retrieval Algorithm Theoretical Basis, available at: http://eospso.gsfc.nasa.gov/eoshomepage/forscientists/atbd/docs/MISR/atbd-misr09.pdf, 1999.

Dubovik, O., Holben, B., Eck, T. F., Smirnov, A., Y. Kaufman, J., King, M. D., Tanré, D., and Slutsker, I.: Variability of absorption and optical properties of key aerosol types observed in worldwide locations, J. Atmos. Sci., 59, 590–608, 2002.

Dubuisson, P., Buriez, J. C., and Fouquart, Y.: High spectral resolution solar radiative transfer in absorbing and scattering media: Application to the satellite simulation, J. Quant. Spectrosc. Radiat. Transfer, 55, 103–126, 1996.

Dubuisson, P., Giraud, V., Chomette, O., Chepfer, H., and Pelon, J.: Fast radiative transfer modeling for infrared imaging radiometry, J. Quant. Spectrosc. Radiat. Transfer, 95, 201–220, 2005.

Eguchi, N. and Yokota, T.: Investigation of clear-sky occurrence rate estimated from CALIOP and MODIS observations, Geophys. Res. Lett., 35, L23816, doi:10.1029/2008GL035897, 2008.

Frankenberg, C., Hasekamp, O., O'Dell, C., Sanghavi, S., Butz, A., and Worden, J.: Aerosol information content analysis of multi-angle high spectral resolution measurements and its benefit for high accuracy greenhouse gas retrievals, Atmos. Meas. Tech., 5, 1809–1821, doi:10.5194/amt-5-1809-2012, 2012.

Guerlet, S., Butz, A., Schepers, D., Basu, S., Hasekamp,O. P., Kuze, A., et al.: Impact of aerosol and thin cirrus on retrieving and validating XCO_2 from GOSAT shortwave infrared measurements, J. Geophys. Res Atmos., 118, 4887–4905, doi:10.1002/jgrd.50332, 2013.

Hansen, J. and Travis, L.: Light scattering in planetary atmospheres, Space Sci. Rev., 16, 527–610, 1974.

Hasekamp, O. P. and Landgraf, J.: Retrieval of aerosol properties over the ocean from multispectral single-viewing-angle measurements of intensity and polarization: Retrieval approach, information content, and sensitivity study, J. Geophys. Res., 101, D20207, doi:10.1029/2005JD006212, 2005.

Herbin, H., Labonnote, L. C., and Dubuisson, P.: Multispectral information from TANSO-FTS instrument – Part 1: Application to

greenhouse gases (CO_2 and CH_4) in clear sky conditions, Atmos. Meas. Tech., 6, 3301–3311, doi:10.5194/amt-6-3301-2013, 2013.

Ignatov, A.: Sensitivity and information content of aerosol retrievals from the Advanced Very High Resolution Radiometer: radiometric factors, Appl. Optics, 41, 991–1011, 2002.

Klüser, L., Martynenko, D., and Holzer-Popp, T.: Thermal infrared remote sensing of mineral dust over land and ocean: a spectral SVD based retrieval approach for IASI, Atmos. Meas. Tech., 4, 757–773, doi:10.5194/amt-4-757-2011, 2011.

Klüser, L., Kleiber, P., Holzer-Popp, T., and Grassian, V. H.: Desert dust observation from space – Application of measured mineral component infrared extinction spectra, Atmos. Environ., 54, 419–427, 2012.

Kuze, A., Suto, H., Nakajima, M., and Hamazaki, T.: Thermal and near infrared sensor for carbon observation Fourier-transform spectrometer on the Greenhouse Gases Observing Satellite for greenhouse gases monitoring, Appl. Optics, 48, 6716–6733, 2009.

Lebsock, M. D., L'Ecuyer, T. S., and Stephens, G. L.: Information content of near-infrared spaceborne multiangular polarization measurements for aerosol retrievals, J. Geophys. Res., 112, D14206, doi:10.1029/2007JD008535, 2007.

L'Ecuyer, T. S., Gabriel, P., Leesman, K., Cooper, S. J., and Stephens, G. L.: Objective assessment of the information content of visible and infrared radiance measurements for cloud microphysical property retrievals over the global oceans. Part I: Liquid clouds, J. Appl. Meteor. Climatol, 45, 20–41, 2006.

Mishchenko, M. I., Geogdzhayev, I. V., Cairns, B., Rossow, W. B., and Lacis, A. A.: Aerosol retrievals over the ocean by use of channels 1 and 2 AVHRR data: sensitivity analysis and preliminary results, Appl. Optics, 38, 7325–7341, 1999.

Moody, E. G., King, M. D., Schaaf, C. B., and Platnick, S.: MODIS-derived spatially complete surface albedo products: Spatial and temporal pixel distribution and zonal averages, J. Appl. Meteor. Climatol., 47, 2879–2894, 2008.

Oshchepkov, S., Bril, A., Yokota, T., Wennberg, P. O., Deutscher, N. M., Wunch, D., et al.: Effects of atmospheric light scattering on spectroscopic observations of greenhouse gases from space. Part 2: Algorithm intercomparison in the GOSAT data processing for CO2 retrievals over TCCON sites, J. Geophys. Res. Atmos., 118, 1493–1512, doi:10.1002/jgrd.50146, 2013.

Peyridieu, S., Chédin, A., Capelle, V., Tsamalis, C., Pierangelo, C., Armante, R., Crevoisier, C., Crépeau, L., Siméon, M., Ducos, F., and Scott, N. A.: Characterisation of dust aerosols in the infrared from IASI and comparison with PARASOL, MODIS, MISR, CALIOP, and AERONET observations, Atmos. Chem. Phys., 13, 6065–6082, doi:10.5194/acp-13-6065-2013, 2013.

Pierangelo, C., Chédin, A., Heilliette, S., Jacquinet-Husson, N., and Armante, R.: Dust altitude and infrared optical depth from AIRS, Atmos. Chem. Phys., 4, 1813-1822, doi:10.5194/acp-4-1813-2004, 2004.

Pierangelo, C., Mishchenko, M., Balkanski, Y., and Chédin, A.: Retrieving the effective radius of Saharan dust coarse mode from AIRS, Geophys. Res. Lett., 32, L20813, doi:10.1029/2005GL023425, 2005.

Quan, X., Huang, H.-L., Zhang, L., Weisz, E., and Cao, X.: Sensitive detection of aerosol effect on simulated IASI spectral radiance, J. Quant. Spectrosc. Radiat. Transfer, 122 214–232, 2013.

Razavi, A., Clerbaux, C., Wespes, C., Clarisse, L., Hurtmans, D., Payan, S., Camy-Peyret, C., and Coheur, P. F.: Characterization of methane retrievals from the IASI space-borne sounder, Atmos. Chem. Phys., 9, 7889–7899, doi:10.5194/acp-9-7889-2009, 2009.

Remer, L. A., Kaufman, Y. J., Tanré, D., Mattoo, S., Chu, D. A., Martins, J. V., Li, R. R., Ichoku, C., Levy, R. C., Kleidman, R. G., Eck, T. F., Vermote, E., and Holben, B. N.: The MODIS Aerosol Algorithm, Products, and Validation, J. Atmos. Sci., 62, 947–973, 2005.

Rodgers, C. D.: Inverse Methods for Atmospheric Sounding: Theory and Practice, World Sci., Hackensack, NJ, 2000.

Rothman, L. S., Gordon, I. E., Barbe, A., Chris Benner, D., Bernath, P. F., Birk, M., et al.: The HITRAN 2008 molecular spectroscopic database, J. Quant. Spectrosc. Radiat. Transfer, 110, 533–572, 2009.

Schmidt, U. and Khedim, A.: In situ measurements of carbon dioxide in the winter arctic vortex and at midlatitudes: An indicator of the "Age" of the stratosphere, Geophys. Res. Lett., 18, 763–766, 1991.

Scott, N. A.: A direct method of computation of transmission function of an inhomogeneous gaseous medium: description of the method and influence of various factors, J. Quant. Spectrosc. Radiat. Transfer, 14, 691–707, 1974.

Stamnes, K., Tsay, S., Wiscombe, W., and Jayaweera, K.: Numerically stable algorithm for discrete-ordinate-method radiative transfer in multiple scattering and emitting layered media, Appl. Optics, 27, 2502–2509, 1988.

Sutherland, R. and Khanna, R.: Optical properties of organic based aerosols produced by burning vegetation, Aerosol Sci. Technol., 14, 331–342, 1991.

Tanré, D., Herman, M., and Kaufman, Y.: Information on aerosol size distribution contained in solar reflected spectral radiances, J. Geophys. Res., 101, 19043–19060, 1996.

Uchino, O., Kikuchi, N., Sakai, T., Morino, I., Yoshida, Y., Nagai, T., Shimizu, A., Shibata, T., Yamazaki, A., Uchiyama, A., Kikuchi, N., Oshchepkov, S., Bril, A., and Yokota, T.: Influence of aerosols and thin cirrus clouds on the GOSAT-observed CO_2: a case study over Tsukuba, Atmos. Chem. Phys., 12, 3393–3404, doi:10.5194/acp-12-3393-2012, 2012.

Veefkind J. P., de Leeuw, G., Durkee, P. A., Russell, P. B., Hobbs, P. V., and Livingston, J. M.: Aerosol optical depth retrieval using ATSR-2 data and AVHRR data during TARFOX, J. Geophys. Res., 104, 2253–2260, 1999.

Veihelmann, B., Levelt, P. F., Stammes, P., and Veefkind, J. P.: Simulation study of the aerosol information content in OMI spectral reflectance measurements, Atmos. Chem. Phys., 7, 3115–3127, doi:10.5194/acp-7-3115-2007, 2007.

Volz, F.: Infrared optical constants of ammonium sulfate, sahara dust; volcanic pumice and flyash, Appl. Optics, 12, 564–568, 1973.

Yoshida, Y., Ota, Y., Eguchi, N., Kikuchi, N., Nobuta, K., Tran, H., Morino, I., and Yokota, T.: Retrieval algorithm for CO_2 and CH_4 column abundances from short-wavelength infrared spectral observations by the Greenhouse gases observing satellite, Atmos. Meas. Tech., 4, 717–734, doi:10.5194/amt-4-717-2011, 2011.